Two-Dirnensional Pattern Forrnation in *C 0* Oxidation on Pt(100)

D. Lima* and R. F. S. Andrade
Instituto de Fisica, Universidade Federal da Bahia
40210-340, *Salvador, BA, Brazil*

Received June **20, 1994**

The formation of two-dimensional patterns during oxidation on Pt(100) is investigated by numerical integration of a system of four reaction-diffusion equations. The results show the presence of the experimentally observed travelling waves of target type for the inhomogeneous surface. Depending on the value of the diffusion coefficients, the homogeneous surface may exhibit uniform oscillating or static Turing patterns.

I. Introduction

The identification of dissipative structures[1] in open systems as their steady states when driving forces bring them far from thermodynamical equilibrium is certainly a milestone in the investigation of complex systems[2]. The emergence of long-range patterns (temporal, spatia1 or spatiotemporal) appears as a cooperative phenomenon resulting from the short-range local interaction among the very large number of components of such systems. Chemical systems have played a decisive role in this development, since the early discussions by Turing[3], the experimental observation of the Belousov-Zhabotinski reaction[4] and the theoretical works of Prigogine and co-workers[5].

In those investigations it was soon recognized that the presence of a catalytic step in the reaction chain was a necessary condition for emergence of dissipative structures in homogeneous systems. Latter on, dissipative structures were also observed in a very large number of reaction systems which include the presence of heterogeneous catalysts. Among them, the *CO* oxidation on Pt catalysts (monocrystals or dispersed Pt on inert supports) is certainly the most studied system which displays such complex behavior[6–8]. The major reason underlying this particular interest lies in the simplicity of the system, as regards both the catalyst structure and reaction products. For Pt monocrystals operating in ultra-high vacuum conditions, it has been possible to identify that a dynamical coupling between the crystalline structure of the surface and the chemical kinetics is the driving mechanism for the formation of temporal and spatial structures[9–11]. This identification has been confirmed by the analysis of the outlet records and by the use of the most advanced techniques in the analysis of surfaces, as standard LEED and work function[10], scanning LEED[9], scanning photoemission microscopy (SPM)[12], and photoemission electron microscopy (PEEM)[13,14]. They show a clear correlation between the reaction product outlets and the changes in surface structure. Moreover they also show the formation of travelling waves on the catalyst's surface[9], whose peaks and valleys indicate different surface properties (crystalline structure, catalytic activity and so on).

The purpose of this work is to further proceed with our theoretical investigations on the occurence of complex behavior during the *CO* oxidation on Pt(100)

*Present address: Service de Chimie-Physique, Center for Nonlinear Phenomena and Complex Systems, CP 231, Université Libre de Bruxelles, 1050, Bruxelles, Belgium; e-mail: dlima@ulb.ac.be
te-mail: fis473@brufba.bitnet

monocrystals[15–18]. We present a discussion on the formation of two-dimensional dissipative structures in the very low presence regime ($P_{CO}, P_O \sim 10^{-9} - 10^{-3}$ Torr). Our study is based on a system of four coupled reaction-diffusion equations which has been introduced to analyze both the homogeneous and the one-dimensional space dependent situations. In our previous works we have shown that this model is able to reproduce the major features of the CO oxidation on Pt(100) which have been experimentally observed: the presence of an oscillatory region in the (P_{CO} x P_O partial pressures diagram, which quantitatively agrees with experimental data[10,16]; the presence of trigger waves when the surface itself is not homogeneous[17,20]. Finally the formation of static Turing structures has been predicted, provided one of its diffusion coefficients could be larger than its typical actual value[21]. The analysis of the two-dimensional surface is motivated by the need for a description of the actual situation on the catalyst surface and by the richness of different patterns (static or dynamical) which can occur in two-dimensional systems[22].

The rest of the paper is so organized as: in Sec. II we present the model and discuss its major features in the context of experimental observations. Also, we comment on the stability diagram, which is the same obtained for the one-dimensional study. In Sec. III we discuss the integration of the system when the surface is homogeneous, in particular the emergence of static Turing structures. In Sec. IV we consider the situation where the surface is inhomogeneous. It is well known from the analysis of other similar systems that inhomogeneities may give rise to the formation of trigger and spiral waves, and we discuss their presence in our model. Finally, Sec. V closes the paper with concluding remarks and suggestions.

II. The model

The Pt(100) surface may exist with two different crystalline structures: hexagonal (hex) and 1 x 1, where the surface atoms have the same symmetry as in the bulk[10]. The 1 x 1 arrangement constitutes the catalytic active phase, where both CO and O_2 adsorb and react, while only CO adsorbs in the (catalytic inert) hex phase. The clean 1 x 1 phase is unstable, thus the surface changes into the hex phase if it is free from adsorbed species. This situation can be reversed if CO molecules adsorb on this phase. This switching back and forth between catalytic and inert surface phases, due to the dynamical interaction among gas molecules and the surface itself, is actually the driving mechanism for the observed complex behavior of the system. This link has been experimentally verified by direct observation of the surface and measurements of the oulet reaction products[10]. The reaction proceeds in the 1×1 phase according to the Langmuir-Hinshelwood mechanism. The O_2 molecules adsorb dissociatively, with very large adsorption heat, being bounded to a fixed surface site. Thus it suffers the influence of the preadsorbed species. On the other hand, the CO molecules are loosely physisorbed and may diffuse (in a macroscopic sense) along the surface. Moreover, their binding energy to a hex site is smaller than that to a 1×1 site. So a trapping mechanism is of relevance, where a CO adsorbed on a hex site migrates (in a microscopic sense) to a neighboring empty 1 x 1 site[19]. All these facts are taken into account by the following system of reaction-diffusion equations:

$$\frac{\partial u_a}{\partial t} = a k_1 P_{CO} - k_2 u_a + k_3 a u_b - k_4 \frac{u_a v_a}{a} + k_5 \nabla^2 u_a \ , \tag{1}$$

$$\frac{\partial u_b}{\partial t} = (1-a) k_1 P_{CO} - k_6 u_b - k_3 a u_b \ , \tag{2}$$

$$\frac{\partial v_a}{\partial t} = a k_7 P_{O_2} \left[\left(1 - \frac{s v_a}{a} - \frac{r u_a}{a} \right)^2 + \alpha \left(1 - \frac{s v_a}{a} \right)^2 \right] - k_4 \frac{u_a v_a}{a} \ , \tag{3}$$

and

$$\frac{\partial a}{\hat{a}t} = k_8 \left[\frac{u_a + v_a}{a} - \bar{\eta}_2 a - \bar{\eta}_3 a^2 - \bar{\eta}_4 a^3 \right] + k_9 \nabla^2 a \tag{4}$$

The space- and time- dependent variables u_a, u_b, v, and a describe, respectively, the fraction of 1×1 and hex sites occupied by adsorbed CO, the fraction of 1×1 sites occupied by O atoms, and the fraction of all surface sites which are in the 1 x 1 phase. k_1, k_2, k_6 and k_7 are the rate coefficients for adsorption and desorption, while k_3 and k_4 are the trapping and reaction coefficients. r and s describe the inhibition in the adsorption of O_2 due to presence of pre-adsorbed CO and **O.** Enhancement on O_2 adsorption comes from the presente of surface defects, and this effect is included in the model through the parameter α. While the first three equations were entirely derived from the observed kinetics, Eq.(4) has been derived from a site interaction model, as

$$\int_S \rho \frac{\partial a}{\partial t} dS = -k_8 \frac{1}{\epsilon_1} \frac{\delta g_{GL}}{\delta a} , \tag{5}$$

where p indicates the density of active sides on the surface and g_{GL} indicates the Ginzburg-Landau potential, which approximates the free energy of the surface:

$$g_{GL} = \int_S \rho \left[-\epsilon_1 \theta_a a + \eta_2 a^2 + \eta_3 a^3 + \eta_4 a^4 + \frac{k_9}{2} (\nabla a)^2 \right] dS . \tag{6}$$

We omit here a discussion on the details of the site model and of the derivation of (6) (see [16] and [17]), but we recall that the $\bar{\eta}_i$, in (4) are closely related, through derivatives, to the η_i coefficients of g_{GL}. We also remark the presence of η_3 in (6), which is characteristic for the description of first order phase transitions, as actually occurs with the hex $\leftrightarrow$ 1 x 1 transition under consideration.

All rate coefficients for the chemical steps of the model are quite well known from experiment. On the other hand, the coefficients of g_{GL} were obtained from the parameters which are present in the site interaction model. Their values were derived through comparison with the measured adsorption heat and by tuning two free parameters to quantitatively reproduce a typical histeresis loop in the CO adsorption and desorption on Pt(100)[23]. Table 1 shows the values of all coefficients in equations (1)-(4) (system S1). We observe in Table 1 that $k_4 \approx 10^5$ and $k_3 = 50$. These two coefficients are related to the eigenvalues of the linear stability analysis of the fixed points of the model as $\lambda_1 \approx -k_4$, $\lambda_2 \approx -(ak_3 + k_6) \approx -10^2$. This indicates that the dynamics of the model along the direction of the corresponding eigenvectors is of the fast relaxing type. So we may make an adiabatic elimination of the fast relaxing modes to reduce the original model to a system of two equations[16]:

Table 1

Constants	Value in this work
k_1	2.5×10^5 ML s^{-1} $torr^{-1}$
k_2	1 s^{-1}
k_3	50 s^{-1}
k_4	$10^2 - 10^5$ ML $torr^{-1}$
k_5	$10^{-4} - 10^{-3}$ $cm^2 s^{-1}$
k_6	10 s^{-1}
k_7	5.6×10^4 ML s^{-1} $torr^{-1}$
k_8	1 s^{-1}
k_9	$10^{-4} - 10^{-1}$ cm^2 s^{-1}
$\bar{\eta}_2$	4
$\bar{\eta}_3$	-10
$\bar{\eta}_4$	7
r	1.6
s	5/3

$$\frac{\partial \omega}{\partial t} = ak_1 P_{CO}\frac{1+q}{1+aq} - k_2\frac{(\omega+|\omega|)}{2} + \Theta(\omega)k_5\nabla^2\omega - ak_7 P_{O_2}\left[\left(1-\frac{(r-s)\omega+(r+s)|\omega|}{2a}\right)^2 + \alpha\left(1-\frac{s(\omega-|\omega|)}{2a}\right)^2\right] \quad (7)$$

and

$$\frac{\partial a}{\partial t} = k_s\left[\frac{|\omega|}{a} - \bar{\eta}_2 a - \bar{\eta}_3 a^2 - \bar{\eta}_4 a^3\right] + k_9\nabla^2 a\ , \quad (8)$$

where $w = u_a - v$, $+aqu_b/(1+aq)$, $q = k_3/k_6$ and $\Theta(\omega)$ indicates the Heaviside function. The system (7)-(8) (system S2) is very useful since it reproduces almost the same dynamics as S1, with the advantage of reducing the computing times by about half. We also note a large difference between the two diffusion coefficients $k_5 \sim 10^{-5} - 10^{-7} cm^2 s^{-1}$ and $k_9 \sim 10^{-15} cm^2 s^{-1}$. As we have already mentioned, the value of k_5 has been experimentally measured, while that of k_9 is obtained from the site interaction model. Its very small value may explain the lack of any experimental result which would require its presence, and perhaps it may actually be neglected in the description of real samples. Nevertheless, its presence enlarges the possibility of novel solutions (as the presence of Turing structures which we discuss in the next section) if we vary its value to explore other regions in the parameter space. While it is true that no such structures have been detected in connection with Pt(100), it is worthwhile mentioning that they have been observed in the CO oxidation on Pt(110)[21], so that the understanding of the relation between this mechanism and the emergence of Turing structures in Pt(100) may help the theoretical investigation of Pt(110). Finally, we stress that the linear stability analysis for the one- and two-dimensional surfaces are the same. Indeed, as shown in [17], the eigenvalues of the stability matrix depend only on the value of $\kappa^2 = |\vec{\kappa}|^2$, where $\vec{\kappa}$ is the wave vector of the perturbation superimposed to the fixed point solution. While we may thus skip this investigation (see [17] for details), we show a typical stability diagram in Fig. 1, where $p_C = 2rk_1 P_{CO}$ and $p_O = 2rk_7 P_{O_2}$. It contains the diagram for space-independent ($k_5 = k_9 = 0$) as well as for space-dependent situation. We observe that the space-dependent diagram was obtained with non-realistic value of $k_9 (k_9 > k_5)$. If we use its typical value, the diagram is coincident with that for the space-independent case.

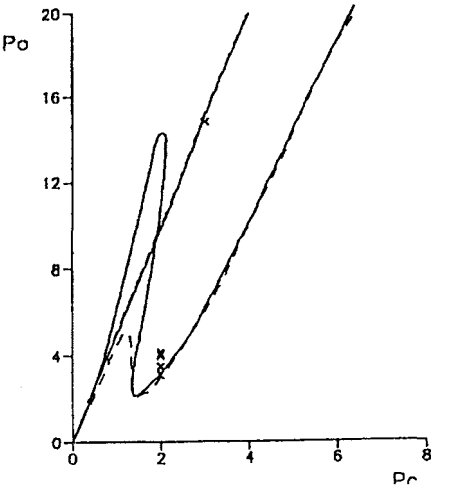

Figure 1: Stability diagram in the partial-pressure plane, with indication of the homogeneous (dashed) (solid-line) and space-dependent ($k_5 = 0.001$, $k_9 = 0.1$) boundaries. The cross indicates the location of the parameters used for the solutions shown in Figs. 2-4.

III. The homogeneous surface

The results discussed in this section refer to the situation where the properties of each site on the surface are

the same. Thus the space and time modulation resulting from the integration of the systems S1 and S2 are solely due to intrinsic instability of the corresponding static and homogeneous branch solution. The systems S1 and S2 were numerically integrated using a finite difference method where the Laplacian is usually approximated by a first order scheme. The sample was divided into a maximal number of 40 cells in each direction. The time dependence has been treated by a fourth-order Runge-Kutta routine and also by the modified Euler method. Both methods are rather stable and give rise to the same solution. We gave preference to the modified Euler method since it is somewhat faster ($\sim$ 30% – 40%) than the Runge-Kutta. The integration was performed on an IBM3090 with vector facility and also on a IBM Risc6000 station. The initial conditions were chosen to be constant values for all cells superimposed to either periodic perturbation or random fluctuations, with no flux through the boundaries of the (finite) sample.

While the actual experimental values of the rate constants are given in Table 1, in the integrations of the systems S1 we have taken a much smaller value for $k_4(10^2)$, otherwise the time step for the integration becomes very small. This change brings no qualitative changes into the solution, while we avoid a large increase in the CPU time required for the integration. For the same reason we have also used much larger values of the diffusion coefficients. As we have discussed before[17], the qualitatively different behavior predicted by the model depends only upon the ratio of the two diffusion coefficients. By increasing their values simultaneously, it is possible to follow the emergence of space-dependent patterns in a much shorter time scale.

In the first part of our investigation we have considered $k_5 = 10^{-3}$ and $k_9 = 10^{-4}$, so that the solutions are qualitatively the same as those obtained with the realistic values of the diffusion coefficients. Our present results confirm those obtained both from the linear stability analysis and from the numerical integration of the one-dimensional situation: the only stable pattern we found was the in-phase oscillation of the whole surface. This contrasts with the results from cellular automata investigations[25] which indicate the presence of travelling waves even in the homogeneous surface. In our model such patterns emerge only when we assume that there exist inhomogeneities on the surface structure, as will be explored in the next section.

The second diffusion coefficient introduced in our model enables the theoretical investigation of other possible classes of solution. So, if we consider $10^{-3} = k_5 < k_9 = 10^{-1}$, we reach a region of the parameter space where the typical solutions are Turing structures, which are qualitatively distinct from those obtained for the actual values of the diffusion coefficients. This is illustrated in Figs. 2-4, where we show snapshots for the variable u_a. The time evolution of the other variables follow this one, with a phase shift which can be positive or negative. The values chosen for p_C and p_O correspond to three typical and distinct situations. In Fig. 2 we have $(p_C, p_O) = (2, 3.1)$ whose position in the diagram is indicated in Fig. 1. The snapshots show clearly that the system assymptotically approaches stable, static, space modulated Turing structure. The next figure shows what happens when we move inward in the stability diagram. For $(p_C, p_O) = (2, 4.1)$ we have already reached the region where the Turing mode becomes unstable, and the sole stable solution is a uniform oscillating surface which corresponds to a limit cycle in the phase space. We observe that the spatial structure seen in Fig. 3.a remains from the spatially modulated initial conditions, but it is continuosly damped as time passes by Fig. 4 refers to the point $(p_C, p_O) = (2, 4.0)$. In this situation we have an interplay of the Turing and uniform oscillating Hopf modes. While it is difficult to give a quantitative analysis of the situation, we can qualitatively understand that the Turing mode is about to become unstable, while the Hopf cycle is about to become stable if it has not already[17,26]. The resulting picture is that of a periodic cycle which carries along a surface modulated structure.

A comparison of the above results with those obtained for the one-dimensional surface indicates that they are alike. Both follow the same path upon increasing the value of p_O, homogeneous state $\rightarrow$Turing $\rightarrow$ Turing + Hopf $\rightarrow$ Hopf $\rightarrow$ Turing $\rightarrow$ homogeneous

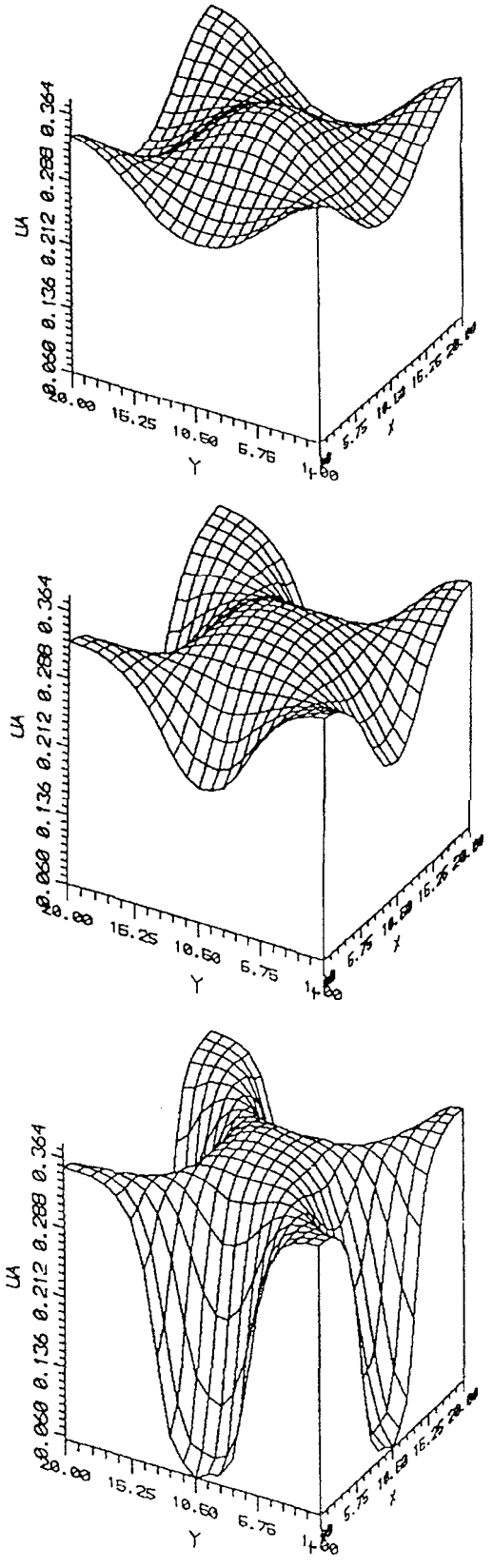

Figure 2: Three snapshots during the formation of a stable Turing structure, taken at t = 0.5s, 8.5s and 20s.

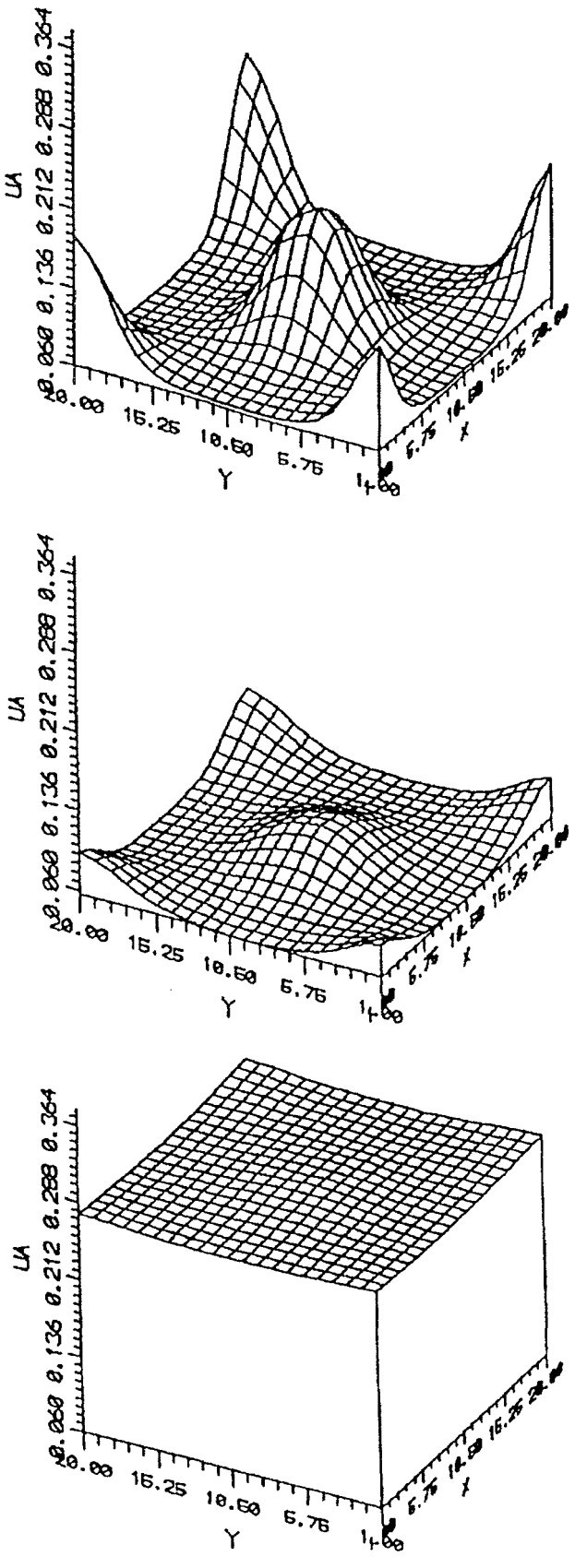

Figure 3: Three snapshots during the evolution of a initially space modulated pattern towards a uniform oscillating surface, at t = 4s, 10s and 19s.

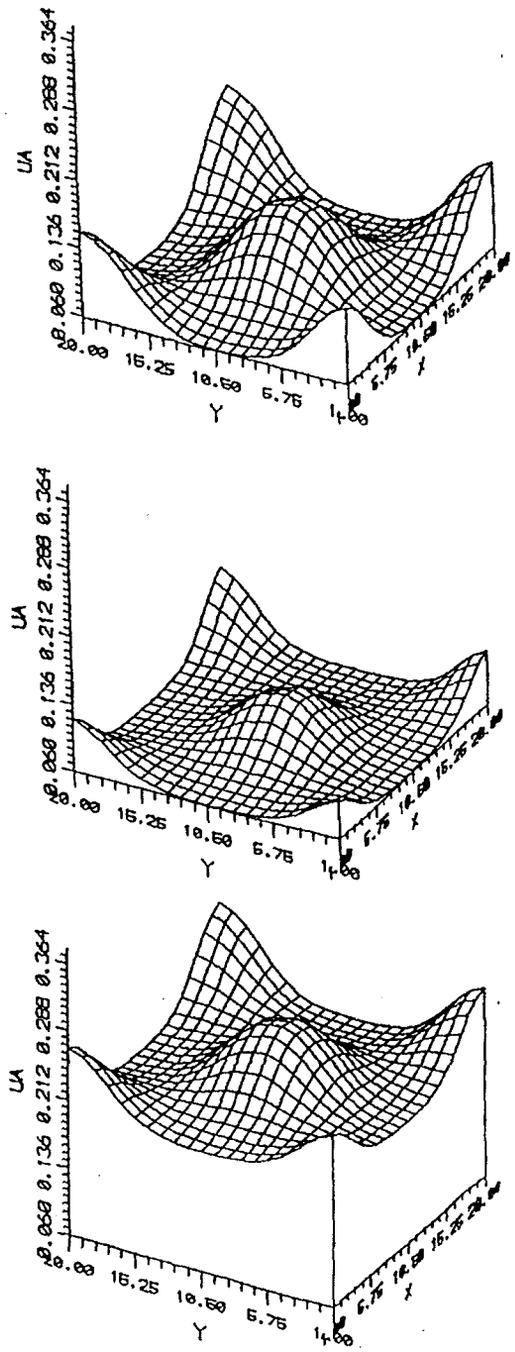

Figure 4: Three snaphots showing the mixed Turing-Hopt mode at $t = 10s, 18s$ and 19s. It is characterized by a in-phase oscillation of a space modulated structure and differs from the typical travelling waves.

state. The last Turing structure we obtain before reaching the instability region has indeed been obtained, although we do not show it here. A competition between Hopf and Turing structures for large values of p_O could not be identified yet, but this may be due to the fact that this region is very small. Several different Turing patterns were also obtained by adequately tuning the initial conditions, e.g. space modulation in only one dimension, or phase shift between x and y directions. As in other problems which also allow for Turing structures, this system must also give rise to other cell structures (hexagonal, circular, etc) if the adequate sample geometry and initial conditions are conveniently chosen[22].

IV. The inhomogeneous surface

The homogeneous surface assumption we considered in the last section can hardly describe the actual experimental situation, even for the very low pressure regimes and the well characterized monocrystal surface experiments we aim to investigate. Indeed, the formation of steps is almost impossible to be inhibited. Also, the process of fixing the sample in the reactor gives rise to an increased formation of defects. While our model already allows for the presence of surface defects, it is natural to ask whether there exist regions on the surface with higher defect rates, and what kind of new effects they bring into the model. This assumption has already been considered in the analysis of the one-dimensional case, where we have shown that the travelling waves can be originated on the sites with higher deffect rates. Our purpose in this section is to investigate the different kinds of wave patterns which can be generated on the two-dimensional surface.

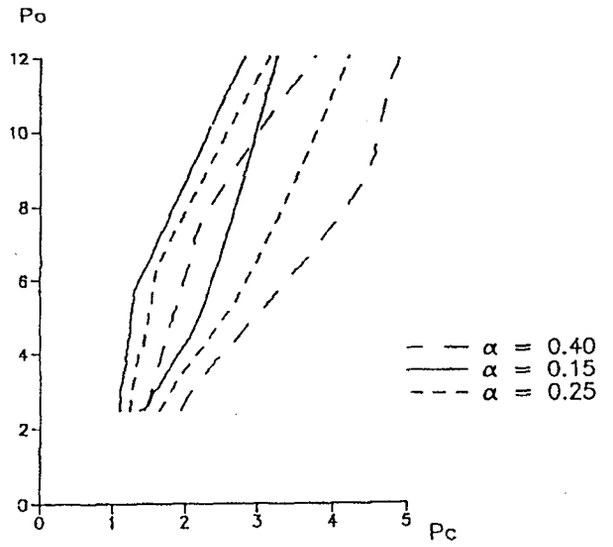

Figure 5: Stability diagrams (as in Fig.1) for different values of k_5 and α. Note the strong dependence on the value of α.

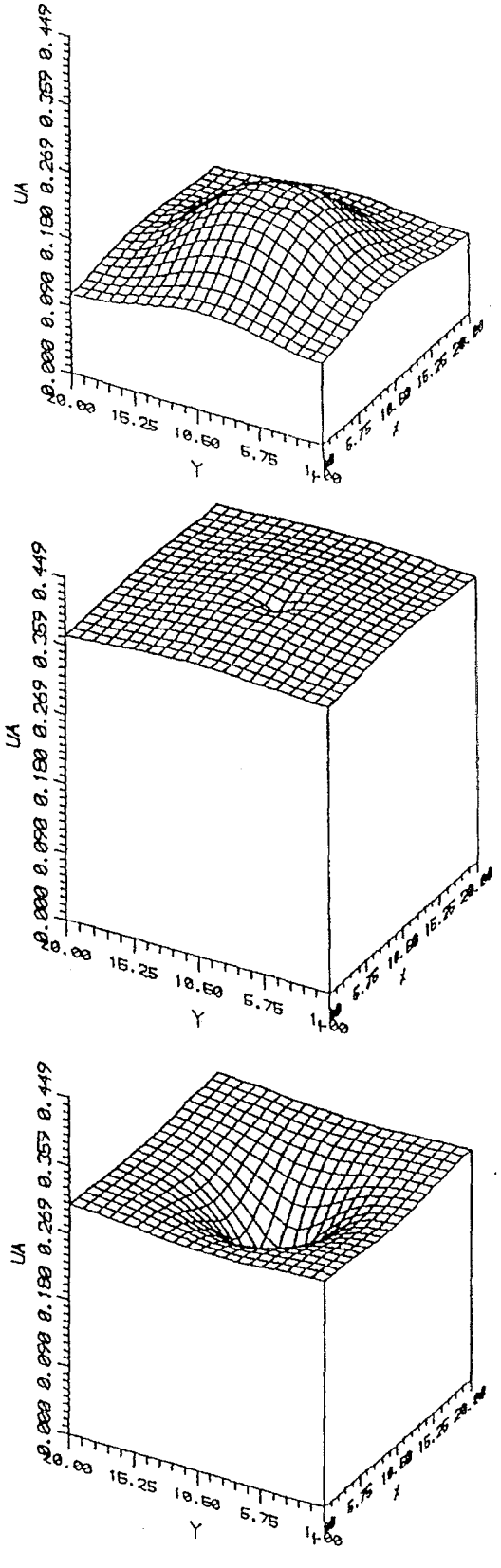

Figure 6: Three snapshots of a target circular wave emerging from a cell with higher defect rate placed in the center of the sample, at $t = 16s, 17$s and 21s.

In what follows we introduce the assumption of surface inhomogeneity, by assigning a higher value of the defect rate parameter a to some isolated sites on the surface. Now we have cells with two different stability properties. As shown in Fig. 5, the stability diagram depends on the value of a. We may have unstable and stable cells, depending on the different values of a which are assigned to them. It can also happen that both of them are unstable, and in this case they will oscillate with different frequencies[17,18]. The coupling of neighboring cells with different dynamic properties through the diffusion coefficients is the generating mechanism of the travelling waves. It is most effective when both α values lie in the instability region. In this situation the higher defect rate cell has a higher frequency and acts as pacemaker for the neighboring cells. Their own eigenfrequency will be enhanced by the presence of a higher frequency cell, but there appears a phase shift between the cells which gives rise to the propagating waves. Damped waves may also occur if the low defect rate cells are stable. In this case the influence of the unstable cells can be restricted to a small region around it. However, this deperids very strongly on the values of the diffusion coefficients and of how stable the other cells are.

The typical results we obtained are shown in Figs. 6a-c, where we have placed the cell with the higher defect rate on the middle of the sample. Since we aim to model the actual physical situation we consider $k_5 = 10^{-3}$ and $k_9 = 10^{-4}$. The three snapshots show very clearly how, starting from a seemingly homogeneous situation, the center cell triggers a symmetrical circular wave which propagates in all directions of the sample. A larger sample may entail a larger number of wave fronts, all of them generated at the same cell. The presence or two or more cells with higher value of a gives rise to a competition between the different pacemakers. This becomes very clear if they are oscillating out of phase.

Spiral waves are a second class of propagating wave pattern which occurs in several reaction diffusion systems[22]. They have not been reported in experiments with $Pt(100)$, but the PEEM analysis shows their presence very clearly in the CO oxidation on

Pt(110)[14]. Also, a recent analysis of the CO oxidation on Pt(100) through cellular automata has reported that such patterns can be generated within the proposed automata rules. Therefore we have also investigated the possible existence of such patterns as solutions of our model. It is well known that the emergence of such patterns depends strongly on the initial conditions, which should display a topological discontinuity along a curve within the surface. Despite the fact that carefully prepared initial conditions have been used, we could not find any stable spiral waves in our model. After an initial interval, where the anisotropic wave front was due to the influence of the initial conditions, the pattern always returned to the symmetrical target wave pattern. Also, the choice of different diffusion coefficients along the x and y directions along the surface does not cause any change in the picture above described, the only exception being that the target fronts become ellipses.

Though the failure in finding spiral waves does not contradict experiment, it certainly uncovers a second difference between the results predicted by the cellular automata method and the integration of the reaction-diffusion equations. This indicates the need for a close comparison between the methods and the different physical assumptions which have been used to model the same situation.

V. Conclusion

In this work we have investigated the emergence of two-dimensional dissipative structures during the CO oxidation on Pt(100), by integrating a system of four coupled partial differential reaction-diffusion equations. The model considered has been previously used with success in the analysis of both the space-independent and the one-dimensional space dependent situations. Our major purpose was to explore the richness of allowed patterns in two-dimensional situations and to compare our results with experiments and theoretical investigations using cellular automata. The results of our investigation corroborate the overall aspects which have been detected in the analysis of the one-dimensional situation, which are rather close to the experimental results. Indeed, we only found travelling wave patterns with the assumption that the surface properties were space dependent, which is actually very close to the experimental situation. The in-phase oscillations observed for the homogeneous surface are very distinct from the observed experimental patterns and should therefore be rejected. The travelling wave patterns we found were of the target types, with circular or elliptic shape depending on the symmetry assumption for the diffusion coefficients. They are the two-dimensional counterpart of the travelling waves reported before. Spiral waves could not be found, though we have made a careful attempt in this direction. This result agrees with experiment, which until now has failed to find such pattern, and contrast with recent results obtained cellular automata. Cellular automata have also indicated the presence of travelling waves in the homogeneous surface. A closer comparison between the actual physical situation described by the two models is therefore necessary to conclude about the reason of such different results. We stress that the fact that the experimental waves start at the sample edges, where the defect rate is known to be greater, favours our results.

Finally, we also explored the emergence of two-dimensional Turing structures, though it does not correspond to a physically possible situation for Pt(100). Our results corroborate those obtained for the one-dimensional surface, though with a richer set of possible patterns. The emergence of one pattern or the other is dictated by initial and boundary conditions, the latter being connected with the sample geometry. Also here we have found the mixed Turing-Hopf mode when we move further into the instability region after crossing its (Turing) border line.

Thus, this work has shown that this model based on reaction-diffusion equations actually reproduces the experimental results, and is a useful tool for the investigation of further aspects of this and other similar situations. As a concluding remark, we point out that the introduction of a second diffusion coefficient in the analysis of the CO oxidation on Pt(110) may be useful for the description of the reported Turing structures.

Acknowledgements

This work was supported by the Brazilian Agencies CAPES and CNPq.

References

1. G. Nicolis and I. Prigogine, *Self-Organization in Noneequilibrium Systems* (Wiley, New York, 1977).
2. G. Nicolis and I. Prigogine, *Exploring Complexity: An Introduction* (Freeman, New York, 1989); also G. Nicolis, Rep. Prog. Phys. 49, 873 (1986).
3. A. M. Turing, Philos. Trans. Royal Soc. London B 327, 37 (1952).
4. B. P. Belousov, Ref. Radiati Med, 1958 Medzig, Moscow, 145 (1959); A. M. Zhabotinskii, Dokl. Akad. USSR 157, 392 (1964).
5. I. Prigogine and G. Nicolis, J. Chem. Phys. 46, 3542 (1967); I. Prigogine and R. Lefever, J. Chem. Phys. 48, 1695 (1968)
6. L. F. Razon and R. A. Schmitz, Catal. Rev. Sci. Eng. 28, 89 (1986).
17. G. Ertl, Science 254, 1750 (1991).
8. R. Imbihl, in *Optimal Structures in Heterogeneous Reaction Systems,* edited by P. J. Plath (Springer, Berlin, 1989), p. 26.
9. M. P. Cox, G. Ertl and R. Imbihl, Phys. Rev. Lett. 54, 1725 (1985).
10. R. Imbihl, M. P. Cox and G. Ertl, J. Chem. Phys. 84, 3519 (1986).
11. M. Eiswirth, P. Moller, K. Wetzel, R. Imbihl and G. Ertl, J. Chem. Phys. 90, 510 (1989).
12. H. H. Rotermund, S. Jakubith, A. von Oertzen and G. Ertl, J. Chem. Phys. 91, 4942 (1989).
13. M. E. Kordesll, W. Engel, G. Lapeyere, E. Zeitler and M. Bradsllaw, Appl. Phys. Lett A 49, 399 (1989).
14. S. Jakubith, H. H. Rotermund, W. Engel, A. von Oertzen and G. Ertl, Phys. Rev. Lett. 65, 3013 (1990).
15. R. F. Andrade, in *Spatial Inhomogeneities Behavior in Chemical Kinetics,* edited by P. Gray et. al. (Manchester University, Manchester, 1990), p. 741.
16. R. F. S. Andrade, G. Dewel and P. Borckrmans, J. Chem. Phys. 91, 2675 (1989).
17. R. F. S. Andrade, D. Lima, G. Dewel and P. Borckmans, J. Chem. Phys. 100, 9192 (1994).
18. D. Lima, M.Sc. thesis, Universidade Federal da Bahia, Salvador, Brazil (1993).
19. R. Imbihl, M. P. Cox, G. Ertl, H. Muller and W. Brennig, J. Chem. Phys 83, 1578 (1985).
20. H. H. Rotermund, W. Engel, M. Kordesh and G. Ertl, Nature 343, 355 (1990).
21. J. Falta, R. Imbihl and M. Henzler, Phys. Rev. Lett. 64, 1409 (1990).
22. S. Chandrasekhar, *Hydrodynamic and Hydromagnetic Stability* (Oxford University Press, Oxford, 1961); for recent progresses in this theme see, e.g., *Spontaneous Formation of Space-Time Structures and Criticaly* - NATO ASI Series, edited by T. Riste and D. Sherrington, (Kluwer Academic Publishers, Doordrecht, 1991).
23. P. A. Thiel, R. J. Behm, P. R. Norton and G. Ertl, J. Chem. Phys. 78,7448 (1983); T. E. Jackman, K. Griffiths, J. A. Davis and P. R. Norton, J. Chem. Phys. 79, 3529 (1983).
24. B. Poelsema, S. T. de Zwart and G. Comsa, Phys. Rev. Lett. 49, 578 (1982).
25. P. Moller, K. Wetzel, M. Eiswirtll and G. Ertl, J. Chem. Phys. 85, 5328 (1986).
26. H. Kidachi, Prog. Theor. Phys. 63, 1152 (1980).
27. R. Kapral, A. Lawniczack and P. Masiar, Phys. Rev. Lett. 66, 2539 (1991).